

LIFETIME AND OPERATIONAL CRITERIA OF PROTON BEAM INSTRUMENTATION IN THE ESS TARGET STATION

Y. Lee*, T. Shea, C. Thomas, European Spallation Source ERIC, Lund, Sweden

Abstract

At European Spallation Source, a 2 GeV, 5 MW proton beam will be delivered from a superconducting linear accelerator to the target at 4% duty factor, which poses demanding requirements on the target station design. To avoid a failure of the target station components due to an accidentally anomalous behavior of beam optics, the current density, the halo distribution, and the position of the proton beam shall be measured. The proton beam instrumentation plug (PBIP) provides a suite for the beam monitoring devices that are important for the machine protection, which include the multi-wired grids for the beam profile monitoring, the thermocouple assemblies and the secondary emission blades for the aperture monitoring, and a beam footprint imaging system consisting of the optical components and a luminescent coating. Since these devices are exposed to a high dose of radiation damage and particle energy deposition, it is a significant challenge to ensure its full functionality. In this paper, the material selection, the lifetime and operational criteria of the beam monitoring devices in the PBIP are presented.

INTRODUCTION

The proton beam instrument plug (PBIP) is located at 1.6 m beam upstream from the target beam entrance window (BEW) and at 2.0 m beam downstream from the proton beam window (PBW). Figure 1 shows the location of the PBIP at the ESS target station.

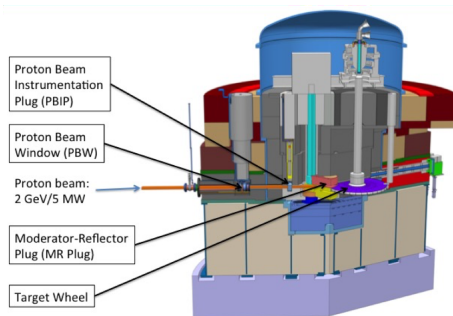


Figure 1: The location of the PBIP in the target monolith.

The PBIP provides a suite for the beam monitoring devices, which include the multi-wired beam profile monitor (MWPM), the secondary emission blades with the thermocouples for the aperture monitoring, and the optical components for the beam footprint imaging at BEW and PBW. The conceptual drawing of the MWPM and the aperture monitor as installed in the PBIP is shown in Fig. 2.

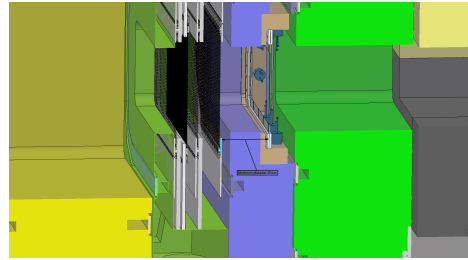


Figure 2: The conceptual drawing of the MWPM and the aperture monitor.

ELECTRON EMISSION YIELD

The multi-wired beam profile monitor (MWBP) and the aperture monitor operate on the net charge deposition in the sensing material, as a result of the secondary electron emission (SEE) and a delta-ray production and transport.

The secondary emission yield (SEY) is defined by the ratio of the number of protons passing through the sensing material to the number of very low energy (less than 1 keV) electrons emitted. The SEY is empirically described by the Sternglass theory [1],

$$SEY = \frac{P \cdot d_s}{E^*} \frac{dE}{dz}, \quad (1)$$

where P is the probability of an electron escaping, d_s is the average depth from which the secondaries arise, E^* is the average kinetic energy lost by the incoming particle per ionization, and dE/dz is the proton stopping power of the wire. The Sternglass parameters we shall use in this paper are $P = 0.5$, $d_s = 1.0 \cdot 10^{-9}$ m and $E^* = 25$ eV.

The electron loss from the sensing material due to delta-ray emission can be calculated by the particle transport code FLUKA [2,3]. The fast electron yield due to the delta-ray emission has been calculated using FLUKA, by counting the net flux of the charged particles cross the surface boundary of the sensing materials. The calculated kinetic energy of the transported high-energy electrons across the wire boundary surface is typically within the range between 10 keV and 1 MeV.

MULTI-WIRED BEAM PROFILE MONITOR (MWPM)

The MWPM consists of five layers of horizontal, vertical, and diagonal wires. It measures the position, profile, and peak density of the high intensity proton beam traveling to the spallation target.

* yongjoong.lee@ess.se

Candidate Materials

For the MWPM wires, tungsten and SiC are widely used at high power H^+ and H^- accelerators. These two materials are considered as the candidate materials for the MWPM wires at ESS. The chosen wire diameter is $100\ \mu\text{m}$, following the MWPM designs at SNS (W, $\phi 100\ \mu\text{m}$) [4], JSNS (SiC, $\phi 100\ \mu\text{m}$) [5], BLIP (W-Re, $\phi 100\ \mu\text{m}$) [6], ISIS (SiC, $\phi 100\ \mu\text{m}$) [7] and LANSCE (SiC, $\phi 79\ \mu\text{m}$) [8].

Electron Emission Yield

Electron Yield by Primary Particles The net charge deposition in the harp wires due to SEY and delta-ray yield (DEY) has been calculated, for an ideal proton beam profile which is calculated by a beam dynamics code. Table 1 shows the calculated electron yields due to SEE and delta-ray emission, respectively for the tungsten and the SiC wire options.

Table 1: Calculated Electron Yields for a 2 GeV H^+ Beam

Wire Material	dE/dz [MeV/cm]	SEY	DEY	Total Yield
Tungsten	24.4	0.049	0.026	0.075
SiC	5.16	0.010	0.013	0.023

The calculation method used for obtaining the result in Table 1 has been applied for calculating the electron yields at the harps at SNS and LANSCE, for a benchmarking. The harp at the upstream of the spallation target at SNS is made of tungsten, which intersects a 1 GeV proton beam. The calculated electron yields due to SEY and DEY from the tungsten wires are respectively 0.049 and 0.028. The total electron yield of 0.077 is in good agreement with the measured quantity 0.07 by 10% [4]. The 1L harp at LANSCE is made of SiC, intersecting an 800 MeV proton beam. The calculated values for the SEY and the DEY are 0.012 and 0.012 respectively, making the total yield 0.024. The calculated electron yield over-estimates the measured value of 0.01 [8] by 140%.

Electron Yield by Primary and Secondary Particles

In reality, the MWPM wires also intersect the secondary particles coming from the shielding blocks surrounding the beam pipe and the PBW. In order to estimate the effect of these secondary particles, the MWPM wires have been modeled in FLUKA in the target monolith environment.

Figure 3 shows the calculated net charge deposition in the horizontal harp wires, due to delta ray production and transport from and to each wire. The 39 wires cover the vertical range of $y \in [-4, 4]$ cm with a 2 mm pitch. For reference, the wire #20 sits at the center of the beam.

Note that the wires in the beam halo region shows the negative net charge deposition. The reason for this is that the electron yield due to the incoming proton beam is balanced out by the incoming secondary electrons to the wires. Figure 4 shows the calculated fast ($E_k > 10$ keV) electron

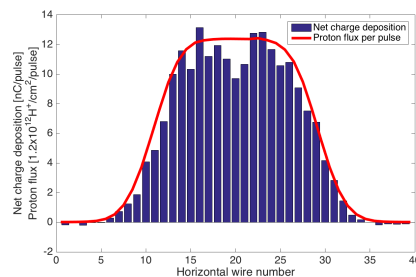


Figure 3: The calculated net charge deposition due to delta-ray production and transport from and to the horizontal harp wires, overlapped with the proton flux projected on the y-axis.

flux configuration in the PBIP region. More than half of the electrons entering the harp wires have kinetic energies below 350 keV, which has a stopping range less than 100 μm range in tungsten.

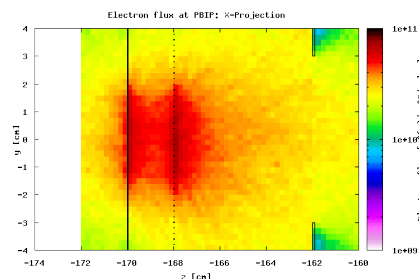


Figure 4: The calculated electron flux configuration in the PBIP region. The vertical and horizontal wires are located at $z = -170$ cm and at $z = -168$ cm respectively. The aperture monitoring blades are located at $z = 162$ cm.

The net charge deposition in the MWPM wires should also take the SEY into account. But, in the halo region, the contribution from the SEY should be smaller than that from the incoming delta-rays, since the ratio of the proton flux to the secondary electron flux decreases. While the slow SEEs can be cleaned by the diagonal biasing wires, the fast delta-rays will overcome the biased electric field.

Radiation Damage

The maximum displacement per atom (dpa) in the wires made of tungsten and SiC are calculated with FLUKA. Table 2 summarizes the maximum calculated dpa rate estimates in the wires for the 5 MW proton beam at ESS.

For comparison, the estimates of the maximum dpa's that have been accumulated in chosen high power H^+ accelerator facilities are calculated, based on the beam parameters and the operational history obtained from the published literature and private communications.

Tungsten wires are used for the beam profile monitoring at SNS. The harp intersects the 1 GeV proton beam with a

Table 2: Calculated Damage Rate Estimates in the Wire for the 5 MW Proton Beam at ESS

Wire Material	Max. dpa Rate [dpa/h]	Annual Operation Time	Max.dpa Rate per Year
Tungsten	0.012	5400	64.8
SiC	0.001	5400	5.4

typical standard deviation of $\sigma_x \times \sigma_y \approx 33 \times 33 \text{ mm}^2$. The accumulated beam power since its commissioning is about 32,000 MWh [9]. Based on this operational information, the maximum damage in the tungsten harp is calculated to be 70 dpa.

The SiC wires are used at JSNS and ISIS-TS2. At JSNS, the harp installed at the PBW intersects the 3 GeV proton beam with a typical standard deviation of $\sigma_x \times \sigma_y \approx 37 \times 17 \text{ mm}^2$. The accumulated beam power for the service period of the first harp system is about 1,900 MWh [10]. Based on this operational information, the maximum damage in the harp at JSNS is calculated to be 0.25 dpa. At ISIS-TS2, the harp made of SiC has been in operation since the commissioning in 2008, without replacement. The harp intersects the 800 MeV proton beam with a beam footprint of $\sigma_x \times \sigma_y \approx 12 \times 12 \text{ mm}^2$. The damage rate in the SiC wire is calculated to be 0.18 dpa/GWh. With the 40 kW beam power at ISIS-TS2, the accumulated beam energy GWh corresponds to 25,000 hours of operation.

Lifetime

Tungsten wire option It is known that the ductile to brittle transition temperature (DBTT) of tungsten increases with the progress of the radiation damage [11]. The high DBTT increases the risk of a brittle failure. As the beam current density at ESS is higher than that of SNS, the tungsten wires at ESS will operate at higher temperatures. At enhanced temperature, the chance of self-annealing of the radiation damage increases. Therefore, it seems to be reasonable to base the lifetime of the ESS harp wires on the maximum accumulated radiation damage of 70 dpa at SNS. The operational lifetime of the harp wires at ESS is estimated to be about 1 year at 5 MW beam operation.

A tungsten-rhenium alloy is used for the harp at BLIP, which intersects the H^- beam up to the kinetic energy of 200 MeV [6]. The fixed harp system at BLIP has reported a failure of the wires in the intensive beam region within a couple of years of operation. The reason for this earlier failure compared to the tungsten harp at SNS could be that the DBTT of the W-Re alloy increases more rapidly with a progressive radiation dose compared to that of pure tungsten [11].

SiC wire option The radiation damage of 5.4 dpa/year in the SiC wire receiving 5 MW beam at ESS far exceeds the damage level accumulated at JSNS and ISIS-TS2. From the 1L harp operation at LANSCE, a failure in one of the SiC wires is reported [8] within a year after its commissioning.

A dedicated irradiation and PIE program would be needed to identify the material degradation of the SiC under proton beam irradiation and to define a service lifetime of the SiC wires.

APERTURE MONITOR AND THERMOCOUPLE

Material Selection

The primary material choice for the aperture monitor at ESS is nickel, following the operational experiences of PSI. A halo monitor mounted at the direct beam upstream of the collimator-2 (KHE-2) at PSI has been operating for more than two decades, without failure. The halo-monitor at KHE-2 is made of 100 μm thick nickel plate, which is segmented in four quadrants [12]. In addition, a number of thermocouples will be attached to the nickel sheet to measure the temperature imbalance.

Electron Emission Yield

Electron Yield by Primary Particles Table 3 summarizes the calculated electron yields due to SEE and delta-ray emission (DEY), respectively for the beam conditions at PSI (575 MeV) and ESS (2 GeV).

Table 3: Calculated Electron Yields in the Nickel Halo-monitors, for the Beam Conditions at PSI (575 MeV) and ESS (2 GeV)

Facility	dE/dz [MeV/cm]	SEY	DEY	Total Yield
PSI	16.7	0.033	0.023	0.056
ESS	13.6	0.027	0.019	0.046

Electron Yield by Primary and Secondary Particles

Figure 5 shows the calculated net charge deposition in the nickel sheets, due to delta ray production and transport from and to each blade. The 6 nickel sheets covers the horizontal range of $x \in [-10, 10]$ cm.

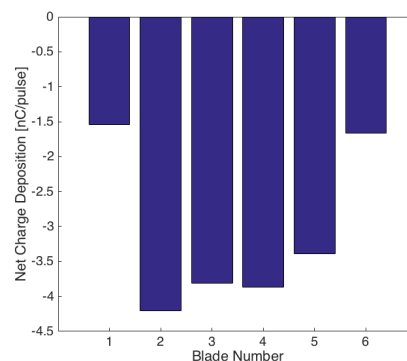


Figure 5: The calculated net charge deposition due to delta-ray production.

The nickel sheets in the beam halo region shows the negative net charge deposition. Majority of the impinging electrons are the delta-rays from the upstream harp wires as seen in Fig. 4. More than half of the electrons entering the harp wires have kinetic energies below 250 keV, which has a stopping range less than 100 μm range in nickel. The electron yield related to Fig. 5 is -0.08 and -0.18 respectively, which out-numbers the SEY of $+0.03$ presented in Table 3. Different from the SEEs, the fast electrons are not cleared by the diagonal wires, which give a voltage bias.

Radiation Damage and Lifetime

The total integrated beam charge since the commissioning of the proton accelerator at PSI as of 2010 is 120 Ah [13]. Based on the beam profile at the Collimator 2, the accumulated maximum radiation damage at the nickel sheet has been calculated with FLUKA. The maximum dpa at the PSI halo-monitor at KHE-2 is about 100.

The dpa in the aperture monitor irradiated by a 5 MW proton beam at ESS has been calculated. The maximum annual dpa accumulation depends on the opening of the aperture monitor. The aperture opening with a maximum damage per year of 10 dpa is roughly defined by $\Delta x \times \Delta y = 12 \times 4 \text{ cm}^2$, for an ideal beam calculated by a beam dynamics code.

CONCLUSION

The electron yields of the harp and the aperture monitoring systems are studied. The charge deposition in the harp and the aperture monitoring blades are due to secondary electron emission and delta-ray production. The secondary charged particles from the shielding blocks, the PBW and the upstream wires attenuate the net charge deposition in the sensing materials. This effect has a major impact on the aperture monitor, which is exposed to the delta-rays produced in the upstream wires. It is therefore recommended to move the aperture monitor to the beam upstream region of the proton beam window.

Further design optimization will be done in the future. Besides the particle transport simulations, the finite-element analyses for the electrostatic, thermal and mechanical characteristics of the sensing systems will be performed, using advanced multi-physics simulation tools. The radiation induced degradation of the sensing material properties will be further investigated, to identify the service lifetime of the beam intersecting systems.

ACKNOWLEDGEMENT

The authors wish to thank Benjamin Cheymol for the help with the use of the FLUKA and Heine Dørlath Thomsen for providing with the seed particle data for the FLUKA simulations. The authors also wish to thank Shin-ichiro Meigo, Willem Blokland, Bryan Jones, Robert

Michnoff and James Sedillo for their generously sharing the operational experiences of the harp systems in their facilities.

REFERENCES

- [1] S. J. Sternglass, "Theory of Secondary Electron Emission by High-Speed Ions", *Physical Review*, vol. 108, no. 1, pp. 1–12, Oct. 1957.
- [2] T. T. Böhlen *et al.*, "The FLUKA Code: Developments and Challenges for High Energy and Medical Applications", *Nuclear Data Sheets*, vol. 120, pp. 211–214, 2014.
- [3] A. Ferrari *et al.*, "FLUKA: a multi-particle transport code", CERN-2005-10, INFN/TC_05/11, SLAC-R-773, 2005.
- [4] W. Blokland, "HIGH BEAM INTENSITY HARP STUDIES AND DEVELOPMENTS AT SNS", in *Proc. 6th Int. Particle Accelerator Conf. (IPAC'15)*, Virginia, USA, May 2015, paper MOAB1, pp. 17–20.
- [5] S. Meigo, M. Ooi, K. Ikezaki, A. Akutsu, S. Sakamoto, and M. Futakawa, "DEVELOPMENT OF PROFILE MONITOR SYSTEM FOR HIGH INTENSE SPALLATION NEUTRON SOURCE", in *Proc. 1st Int. Beam Instrumentation Conf. (IBIC2012)*, Tsukuba, Japan, Oct. 2012, paper MOPB68, pp. 227–231.
- [6] R. Michnoff, Z. Altinbas, P. Cerniglia, R. Connolly, C. Cullen, C. Degen, D. Gassner, R. Hulsart, R. Lambiase, L. Mausner, D. Raparia, P. Thieberger, and M. Wilinski, "THE BROOKHAVEN LINAC ISOTOPE PRODUCTION FACILITY (BLIP) RASTER SCANNING UPGRADE", in *Proc. 3rd Int. Beam Instrumentation Conf. (IBIC2014)*, Monterey, CA, USA, Sep. 2014, paper WEPF26, pp. 608–612.
- [7] B. Jones, private communication, Apr. 2016.
- [8] J. Sedillo, D. Martinez, and J. Nguyen, "LANSCE 1L HARP DATA ACQUISITION SYSTEM UPGRADE: FIRST RESULTS", in *Proc. 4th Int. Beam Instrumentation Conf. (IBIC2015)*, Melbourne, Australia, Sep. 2015, paper TUPB081, pp. 542–546.
- [9] SNS Status, <https://ics-web.sns.ornl.gov/chico/beam.jsp>.
- [10] S. Meigo, private communication, Mar. 2016.
- [11] H. Ullmaier, and F. Carsughi, "Radiation Damage Problems in High Power Spallation Neutron Sources", *Nuclear Instruments and Methods in Physics Research B*, vol. 101, pp. 406–421, 1995.
- [12] U. Rohrer, "The Multilevel Protection System for the Vacuum Chambers of the High-Intensity 590 MeV Proton Beam Lines", PSI Scientific and Technical Report 2003, Volume VI, pp.45–48, 2003.
- [13] Å Strinning, P. Baumann, M. Gandel, D. Kiselev, Y. Lee, and S. Adam, "VISUAL INSPECTION OF A COPPER COLLIMATOR IRRADIATED BY 590 MeV PROTONS AT PSI", in *Proc. of HB2010*, Morschach, Switzerland, Sep. 2010, paper MOPD64, pp. 245–249.